The implications for dust emission modeling of spatial and vertical variations in horizontal dust flux and particle size in the Bodélé Depression, Northern Chad

Adrian Chappell,[1] Andrew Warren,[2] Alice O'Donoghue,[3] Andrea Robinson,[3] Andrew Thomas,[4] and Charlie Bristow[5]

Received 1 June 2007; revised 4 October 2007; accepted 3 December 2007; published 29 February 2008.

[1] The Bodélé Depression has been confirmed as the single largest source of atmospheric mineral dust on Earth. It is a distinctive source because of its large exposure of diatomite and the presence of mega-barchan dunes. Direct measurements of horizontal dust flux and particle size were made to investigate dust emission processes and for comparison with mechanisms of emission assumed in current dust models. More than 50 masts, with traps mounted on each, were located across and downwind of three barchans in 56 km^2 study area of the eastern Bodélé. The size-distribution of surface material is bi-modal; there are many fine dust modes and a mixed mineralogy with a particle density three times smaller than quartz. Horizontal fluxes (up to 70 m above the playa) of particles, up to 1000 μm in diameter, are produced frequently from the accelerated flow over and around the barchans, even in below-threshold shear conditions on the diatomite playa. Our data on dust sizes do not conform to retrievals of dust size distributions from radiance measurements made in the same area. Dust emission models for the region may need to be revised to account for: saltators in the Bodélé, which are a mixture of quartz sand and diatomite flakes; the great spatial and vertical variation in the abundance, mass and density of dust and abraders; and the patterns of surface erodibility. All of these have important local effects on the vertical dust flux and its particle sizes.

Citation: Chappell, A., A. Warren, A. O'Donoghue, A. Robinson, A. Thomas, and C. Bristow (2008), The implications for dust emission modeling of spatial and vertical variations in horizontal dust flux and particle size in the Bodélé Depression, Northern Chad, *J. Geophys. Res.*, *113*, D04214, doi:10.1029/2007JD009032.

1. Introduction

[2] It is widely accepted that the abrasion of the soil surface by saltating quartz sand is the most prolific way in which mineral dust is produced [*Gillette*, 1977]. The rate and spatial variation of dust production derived from the impact of quartz sand saltators are largely controlled both by the erodibility of the surface (surface roughness, aggregate size distribution, surface crusting etc.) and the properties of the saltator. Both are sources of uncertainty in dust emission models. In dune environments, where most saltating grains are quartzose (composed of hard quartz), the saltating grains remain virtually intact on impact and produce very little dust [*Bullard et al.*, 2004]. There are other situations, particularly on agricultural fields, where the saltators are aggregates of smaller-sized material. In this case, most of the saltators and immobile aggregates on the surface disintegrate on impact [*Gomes et al.*, 1990; *Shao and Raupach*, 1993]. The size distribution of the dust produced in this way is a function of the aggregate sizes and the binding energy holding the aggregates together [*Alfaro et al.*, 1997; *Shao and Lu*, 2000; *Alfaro and Gomes*, 2001].

[3] Deserts have an abundance of quartz abraders. *Marticorena et al.* [1997] estimated that approximately 50% of the surface of western Sahara was covered by coarse medium quartzose sand (mean modal diameter = 690 μm). When abundant quartz sand abrader in transport meets fine deposits in dry lakes, 'hot spots' of dust production are created [*Mahowald et al.*, 2003; *Zender et al.*, 2003] and this process is now included in almost all global dust emission models [*Ginoux et al.*, 2001; *Tegen et al.*, 2006; *Miller et al.*, 2006]. Satellite data from the Total Ozone Monitoring Spectrometer (TOMS) have confirmed the Bodélé, a large dry lake in northern Chad, as the most prolific single global source of dust [*Prospero et al.*, 2002]. In recent ground observations of dust emission from the Bodélé, however, there are inconsistencies between estimates of dust production derived from satellite data and those derived from measurements of visibility at ground level [*Washington et al.*, 2003].

[1]Centre for Environmental Systems Research, University of Salford, Manchester, UK.
[2]Department of Geography, University College London, London, UK.
[3]School of Environment & Life Sciences, University of Salford, Manchester, UK.
[4]Department of Environmental and Geographical Sciences, Manchester Metropolitan University, Manchester, UK.
[5]School of Earth Sciences, Birkbeck College, University of London, London, UK.

0148-0227/08/2007JD009032

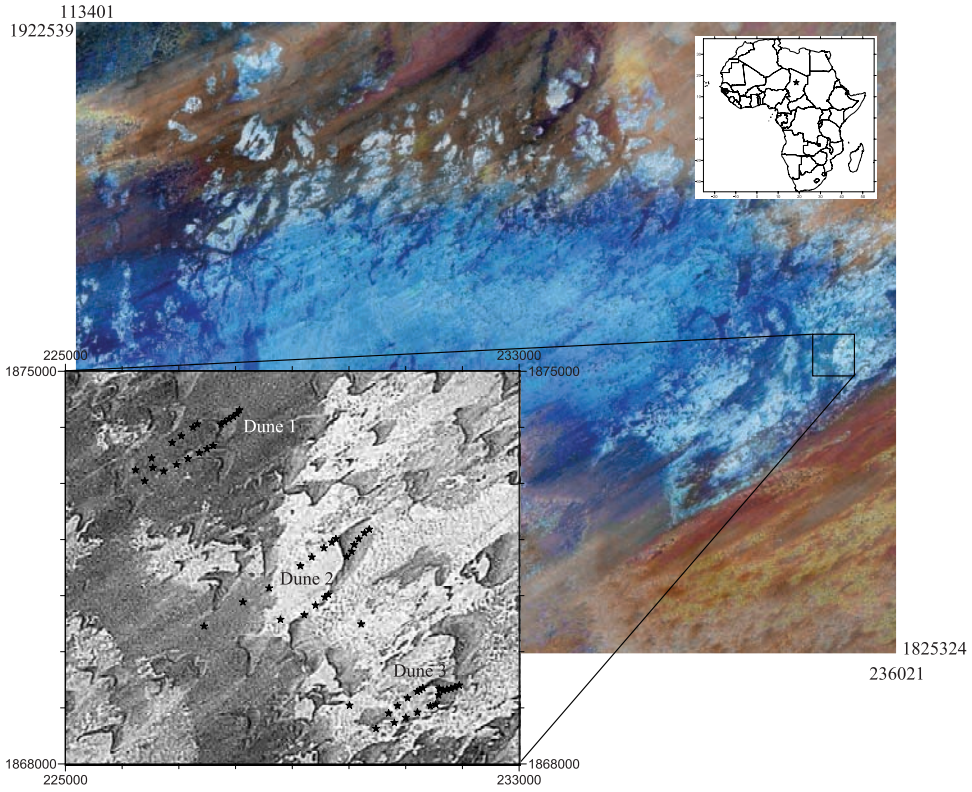

Figure 1. Location of the largest extant area of diatomite (Bodélé Depression) and the study area in Chad. Dust sample locations are identified with * and dune 1 is the northern-most cluster of samples, dune 2 samples are clustered near the center of the image and dune 3 samples are the southern-most samples. Imagery was made available by NASA's Earth Science Enterprise Scientific Data Purchase Program.

[4] A recent estimate of dust produced for the entire 10,800 km^2 of the Bodélé, based on modeling, is 1.2 ± 0.5 Tg day^{-1} [*Todd et al.*, 2007]. This estimate is based on a small number of point measurements (taken at 2 m above the surface) of dust (defined as <10 μm) and surface radiance measurements for several minor events and one major event of approximately 24 h during March 2005 (as described below). The model inversion procedure used to reach these estimates assumed that the aerosol size distribution was homogeneous with height and that it could be extrapolated across the entire Bodélé (on the assumption that dust production and its size distribution were the same throughout the area). Regional model simulations of the Bodélé performed by *Tegen et al.* [2006] estimated total dust emission (between 10–12 March) to be 104 g m^{-2} at one location (Chicha, see below). This estimate is about three times smaller than the comparable estimate of 324 g m^{-2} (±40%) by *Todd et al.* [2007] for the same location and period. *Tegen et al.* [2006] suggested that the discrepancy could be partly explained by the underestimation of maximum wind speeds during days when observed wind speeds exceed 10 m s^{-1} in the model, and the uncertainty of the assumption by *Todd et al.* [2007] that the whole area of diatomite was equally effective in producing dust aerosol (an assumption questioned by *Warren et al.*, 2007).

[5] In this paper we present field data on dust emission from the Bodélé. In particular, we describe strong spatial contrasts in the magnitude and particle size of dust production. Our aim here is to elucidate the processes of dust production and consider the implications for dust emission modeling.

2. Methods

2.1. Study Area

[6] The 56 km^2 study area is near Chicha [UTM 34QBD 238867, 1867971; Figure 1] in the Bodélé Depression in northern Chad, on the south-eastern edge of a large outcrop of freshwater diatomites from the deepest part of now-dry Lake Mega-Chad. The Bodélé is unlike most other dry lakes because its surface comprises a complex mosaic of diatomite outcrops, mega-barchan dunes (crescent-shaped accumulations up to 50 m high) and relict raised channels [*Drake and Bristow*, 2006; *Warren et al.*, 2007] and is exposed to the high wind speeds of the Bodélé Low Level Jet [*Washington and Todd*, 2005; *Washington et al.*, 2006].

[7] An orthorectified Landsat-7 Enhanced Thematic Mapper (ETM+) mosaic scene from the year 2000 shows the setting for the Bodélé Depression and an enlargement of an area dominated by diatomite at the surface (Figure 1). The images are displayed on the UTM projection (WGS84; oriented north; coordinates in meters). The three spectral bands have each been sharpened with the panchromatic band: Band 7 (mid-infrared light) is displayed as red; Band 4 (near-infrared light) is displayed as green; and Band 2 (visible green light) is displayed as blue. The

study area (8 km × 7 km) is displayed on an extract of the mosaics using only Band 4 (NIR). It shows sample locations (see section 2.2 below).

[8] The area of diatomite exposure in the Bodélé is estimated at 10,800 km^2. Diatomite is a silicious, low-density material. It is intercalated with dune sands, presumably reflecting the filling and emptying of the lake during the last three or four thousand years [*Drake and Bristow*, 2006]. Diatomite was deposited when the lake was filled. In dry periods, quartz-sand dunes, driven in by the north-easterly Low Level Jet [LLJ], invaded the lakebed, as they are now again doing [*Warren et al.*, 2007]. The character of the outcrop is diverse, ranging from large areas of massive, compact and off-white diatomite, to limited areas of friable and grey diatomite. Scanning electron microscopy was used to show the nature of the surface material at the toe of a dune (Figure 2; UTM 230700 1872300), which represents material found at similar locations in the study area. Among the rounded quartz grains (up to ca. 1000 μm) are platy fragments (flakes) of diatomite most of which do not exceed ca. 500 μm (Figure 2a). There appears to be no particle aggregation, but almost all the large (quartz) particles have very fine (ca. 10 μm) material attached to them. Intact diatomite particles at this location are around 50 μm in either length or diameter. Much smaller fragments of diatomite appear, with sizes of between 50 μm and 1 μm and smaller (Figure 2b). The diatomites are largely composed of SiO_2 and small quantities of Al_2O_3 and Fe [Table 1]. Because the diatomitic material shown in the figure is attached to many of the large rounded particles it is difficult to separate the elemental makeup of the large particles. However, it is reasonable to suppose that the rounded particles are composed mainly of SiO_2 and $CaCO_3$ but $CaCO_3$ does not occur in the diatomites (Table 1). There are traces of Na, Mg, K and Ca in the rounded particles.

[9] Different surface types in the study area have different erodibilities and therefore make different contributions to dust emission (Figure 1). The compact white diatomite covers large areas of rough topography [Figure 1, UTM 231000, 1872000)] and is the source of white diatomite flakes in accumulations on the ground, which are in various stages of breakdown following aeolian transport, as shown by their rounded edges. Other more friable and darker types of diatomite surface cover much smaller areas and may be

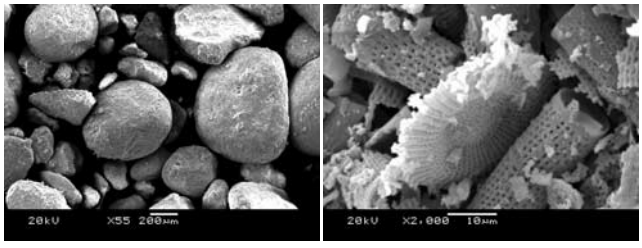

Figure 2. Scanning electron microscope images of material near the toe of dune 2 (UTM 230700, 1872300). The images are taken at (a) 55 times and (b) 2000 times magnification and the scale bars represent 200 μm and 10 μm, respectively. Two species of diatomites are identified from the Frustules and tiny rows of striae as the tubular *Aulacoseira* and discus-like *Stephanodiscus* species.

Table 1. Summary of the X-Ray Diffraction Geochemistry of Material Upwind of Dune 2 (UTM 230700, 1872300)

	Rounded Particles		Diatomite	
Element	*Weight, %*	*Atomic, %*	*Weight, %*	*Atomic, %*
$CaCO_3$	7.48	12.79	...	...
SiO_2	39.74	51.04	34.03	48.70
Na - Albite	1.24	1.10	...	...
MgO	0.74	0.63	...	...
Al_2O_3	5.87	4.47	5.41	4.59
SiO_2	35.96	26.31	53.97	44.01
K - MAD-10 Feldspar	1.35	0.71	...	...
Ca - Wollastonite	0.98	0.50	...	...
Fe	6.66	2.45	6.59	2.70
Totals	100.00		100.00	

remnants of an erodible layer above the compact white diatomite. Accumulations of diatomite flakes also form nabkha dunes which are accumulations around sparse vegetation [Figure 3a]. In other areas there are mega-ripples [up to 30 cm high] built of quartz sand [Figures 3b and 3c]. Pea gravel, composed largely of quartz, is found on extensive surfaces [Figure 3c], perhaps raised channels (exposed by the preferential deflation of the surrounding, finer-grained surfaces) associated with drainage into the lake [*Drake and Bristow*, 2006; *Bristow et al.*, 2008]. The barchan dunes vary in height at the crest from 30 m to 70 m above the diatomite surface [Figure 3d] and each dune typically covers a ground area of approximately 1 km^2 [e.g., Figure 1 230000, 1872000]. The barchans are built of a mixture of sand-sized flakes of diatomite and iron-oxide-coated quartz sand [Figure 3e]. The source for some of the iron is probably nodules exposed on the surface of the underlying floor of the dunes (Figure 3f). The barchan dunes of the study area indicate a dominant north-easterly wind regime [*Washington et al.*, 2006] and the occurrence of small amounts of loose erodible material on top of a hard surface.

2.2. Sampling

[10] The masts to which the sediment traps were attached were cheap and easy to construct, light to transport and sufficiently strong to withstand high wind speeds while also supporting the traps. They were constructed using 4 m lengths of plastic pipe. A 32 mm diameter pipe was inserted up to 1 m on the loose dune surfaces; a 40 mm pipe, with the traps attached, was fed onto it. The outer pipe was bolted to the inner pipe to maintain a constant orientation with the prevailing wind. We constructed Modified Wilson and Cooke Traps (MWACs) [*Wilson and Cooke*, 1980; *Kuntze et al.*, 1989], which was one the most efficient samplers tested by *Goossens and Offer* [2000], and which is in the short-list of samplers recommended by *Zobeck et al.* [2003]. The air inlet pipe of the MWACs has an internal diameter of 11 mm (inlet area ca. 95 mm^2). The MWACs were attached to the masts in a horizontal orientation at 0.75 m, 1.4 m and 2.4 m above the surface.

[11] We expected there to be different amounts of dust emitted from the different surface types, and a sampling strategy was devised that stratified variation within and between the dunes [*Chappell et al.*, 2003a, 2003b]. At approximately 10 locations, the MWACs were attached to the mast in a horizontal orientation at a height of 0.25 m for sampling from within the saltation layer. Approximately

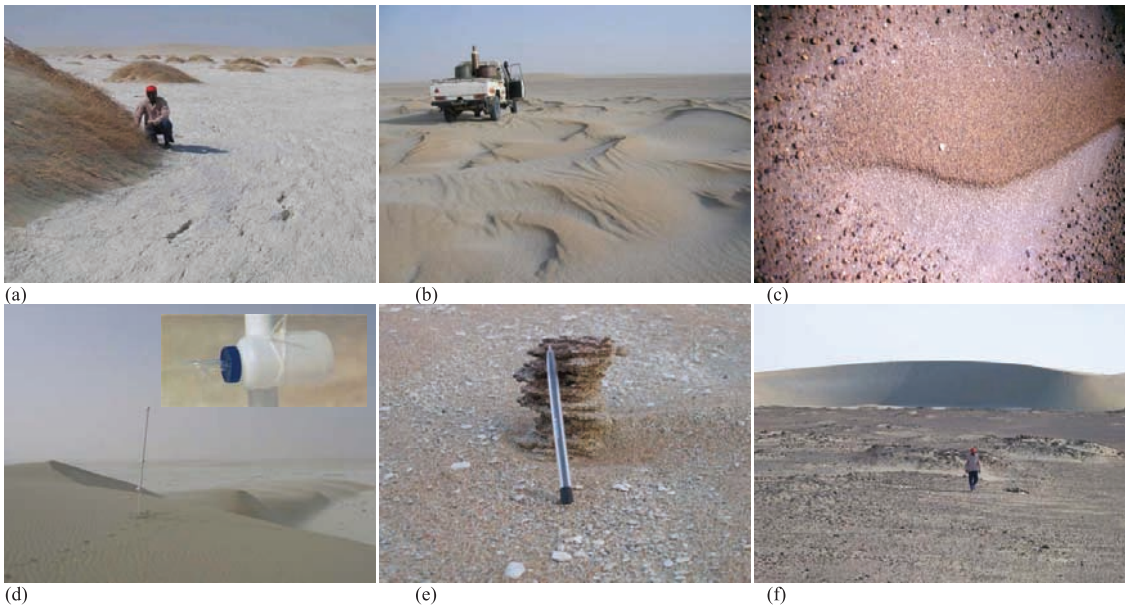

Figure 3. Images of the surface types in the study area: (a) abraded diatomite surface curving around a large (ca. 3 m) nebkha; (b) Mega-ripples of quartz sand; (c) Mega-ripple comprising coarse quartz sand (>1 mm) on the windward flank (darker tones) and diatomite flakes (lighter tones) on the downwind slope and surrounded by rounded pea gravel with approximate equidistant spacing (coin placed on the windward slope for scale); (d) Mega-barchan dune looking toward the southern downwind horn of dune 2 showing a dust trap mast (2.4 m) at the crest (close-up of trap inset); (e) windward slop surface of a barchan dune comprising quartz sand and diatomite flakes. The pedestal (pen displayed for scale) comprises layers of quartz sand from previous wind ward slope surfaces; (f) iron nodules embedded in a quartz sand surface surrounded by barchan dunes.

20 masts were sited on the windward slopes of three barchan dunes to monitor the effect of speedup on dust production. Another ca. 40 masts were placed on transects across the diatomite pavement downwind of these dunes. A few more masts were located between the dunes. The locations of all masts were determined using a handheld global positioning system (GPS) receiver; they are shown superimposed on the satellite imagery (Figure 1). The masts and traps were erected over a period of two days, and were inspected almost every day thereafter in the 10-day field experiment (March, 2005). Most of the horizontal dust flux was produced in an intense storm that lasted about 24 h (10th–12th March, 2005), which had wind speeds at 2 m above the diatomite floor that reached 14 m s^{-1} [*Todd et al.*, 2007]. Daily maximum temperatures fell from 43°C on the 8th March to about 30°C during the major dust storm [*Todd et al.*, 2007]. The traps were not emptied before this storm because emptying so many traps would have been time-consuming and because a large dust event might have been missed in the process. The error introduced by this omission is small, because the quantity of dust trapped before the storm was observed to be very small compared to the amount trapped during the storm. Traps on the masts located between the dunes received no material prior to the storm and were removed and relocated to provide additional detail on the spatial variation of dust production. Unfortunately, during the storm some of the masts were snapped by the wind and others were unearthed. The data from these traps have been omitted from subsequent analysis. During the extreme event, the glass tubes in the traps lying on the dune surface were severely etched by abrasion. A total of 52 locations provided viable measurements of horizontal dust flux for a range of heights above the surface.

[12] In addition to the dust samples, surface samples were taken at the location of those masts (ca. 60 samples), at the intersection of a 1 km regular grid placed over the entire study area (63 samples) and selected locations within the grid (ca. 30 samples) amounting to a total of 153 locations. At locations where material at the surface was unconsolidated, a sample was obtained to a depth of approximately 10 cm using a trowel. At other locations where the surface was consolidated it was broken before sampling.

2.3. Particle Size Measurement

[13] Sediment transport is typically at a maximum at the surface where particles are large, and declines with height as the size of the material decreases. To discover the particular pattern of these relationships in the Bodélé, the material trapped at each height was sieved into two fractions at 63 μm (particle diameter), yielding a "coarse dust" fraction (<63 μm) and a predominantly saltation fraction (>63 μm) (in terms of mass). The choice of this size threshold is based on two main considerations: (i) this size is the easiest for reproducible, and therefore reliable results from sieving; and ii) 63 μm is similar to the upper size limit in many dust emission models [*Gillette*, 1974; *Lu and Shao*, 2001]. To test the hypothesis that sieving through a 63 μm sieve breaks down the diatomite material, replicate samples of dune material were sieved for between 1 and 25 min. Breakdown occurred when the sieving duration exceeded 15 min. This period provided a size-specific mass of sediment transport for each trap, and was therefore chosen

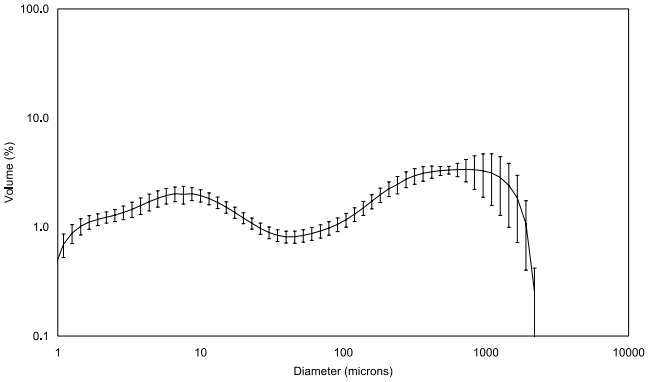

Figure 4. Particle size distribution and error bars representing the standard deviation of 20 re-measured subsamples from dune samples in the study area. Note the logarithmic scale on both axes.

for all subsequent analysis. In addition to this crude separation, we measured a finely resolved particle size distribution (PSD) for samples taken at selected locations. Surface samples and trapped sediment were measured using laser diffraction (LD) with the Mastersizer 2000, in conjunction with that instrument's dry accessory [*Malvern Instruments*, 2003], so that samples could be measured in their field state. Dry measurement was particularly important to retain its field characteristics and because the diatomite material was found to be highly hydrophilic and liable to disperse in a fluid during measurement. In this particle-sizing technique the forward diffraction of a laser beam by the particles determines their size distribution. Mie theory optical modeling is used in the instrument to fit scattering results and interpret angle-dependent scattering by particles. The optimal air pressure for dispersing the samples was determined to be ca. 1.65 bar and was used for all measurements. The LD technique is not sensitive to the refractive index of the material and a value of 1.43 and 0.1 was used for the real and imaginary parts, respectively. During the measurements, the obscuration ratio was maintained between 1% and 5% in keeping with the manufacturer's recommendations and *Chappell* [1998]. The single largest source of variation in measurements of the particle size distribution using LD is sub-sampling [*Chappell*, 1998; *Malvern Instruments*, 2003]. From a bulked sample of dune material taken from the study area, twenty sub-samples were obtained and measured using the settings described above. Figure 4 shows the precision of the instrument and accuracy of re-measurement for those sub-samples. The error bars are the standard deviation of the measurements. The coarsest size fractions contain most variation as a consequence of the number of particles. The average of the standard deviations for all size fractions is 0.22%. Variation in calibration settings was found to be around 0.09% and therefore a lower limit of 0.1% was used to describe the distributions and in considering the occurrences of modes in the size distribution.

2.4. Horizontal Sediment Flux

[14] The horizontal sediment flux at a given height is conventionally defined as the mass of material passing through a given area over a period of time (g m^{-2} s^{-1}). An exponential or power function has been found to fit the distribution with height [*Stout and Zobeck*, 1996]. Although recent work has shown that near the ground those functions do not model the horizontal flux distribution precisely [*Dong et al.*, 2006], they are used here to represent consistently the horizontal flux to an acceptable accuracy, given the sampling limitations. The saltation fraction (>63 μm) of the sediment caught in the traps at each height was divided by the area of the inlet tube and then divided by the duration of the dust event, which was conservatively estimated to be 24 h. To determine the total horizontal saltation fraction flux (integrated saltation flux) at a location, the saltation fraction of the sediment caught in the traps at each height was fitted with the exponential model using least squares regression and that function was integrated between 0 m and 3 m above the surface (x) and divided by the duration of the dust event (g m^{-1} s^{-1}):

$$\int_0^3 ae^{-bx}dx = a\left[\frac{e^{-bx}}{-b}\right]_0^3 + c, \tag{1}$$

where a and b are coefficients of the exponential function and c is the constant of integration.

[15] The mass of the coarse dust fraction (<63 μm) caught in the traps at each height was also divided by the area of the inlet tube and then divided by the same estimate of the duration of the dust event. To determine the total horizontal dust fraction flux (integrated dust flux) at a location, the dust fraction of the sediment caught in the traps at each height was fitted with an exponential model using least squares regression and that function was integrated between 0 m and 3 m above the surface and divided by the duration of the dust event (g m^{-1} s^{-1}). There were several locations at which the vertical profile of the dust fraction did not conform to the expected exponential distribution. At these locations a quadratic polynomial was fitted and integrated between 0 m and 3 m above the surface (x) and divided by the duration of the dust event (g m^{-1} s^{-1}):

$$\int_0^3 a_1x^2 + a_2x + a_3dx = \left[a_1\frac{x^3}{3} + a_2\frac{x^2}{2} + a_3x\right]_0^3 + c, \tag{2}$$

where a_1, a_2 and a_3 are coefficients of the fitted polynomial and c is the constant of integration.

[16] The use of the polynomial is a simplified approximation to recent work [*Butler et al.*, 2005], which explained the departure from a vertical exponential profile as being due to surface heating.

2.5. Surface Classification

[17] Surface samples were classified in a simple system, with regard to their possible influence on the rate of horizontal sediment flux. The samples, still in their plastic bags, were mixed on a flat surface with a light source directly overhead (thus reducing directional illumination effects). The samples were classified according to a visual estimate of their similarity in texture/structure and color. At first, eight classes were defined: (1) material from a quartz barchan outside the study area; (2) fragile grey diatomite (at two locations); (3) mega-ripple quartz material; (4) dune material containing diatomite flakes; (5) rounded/abraded

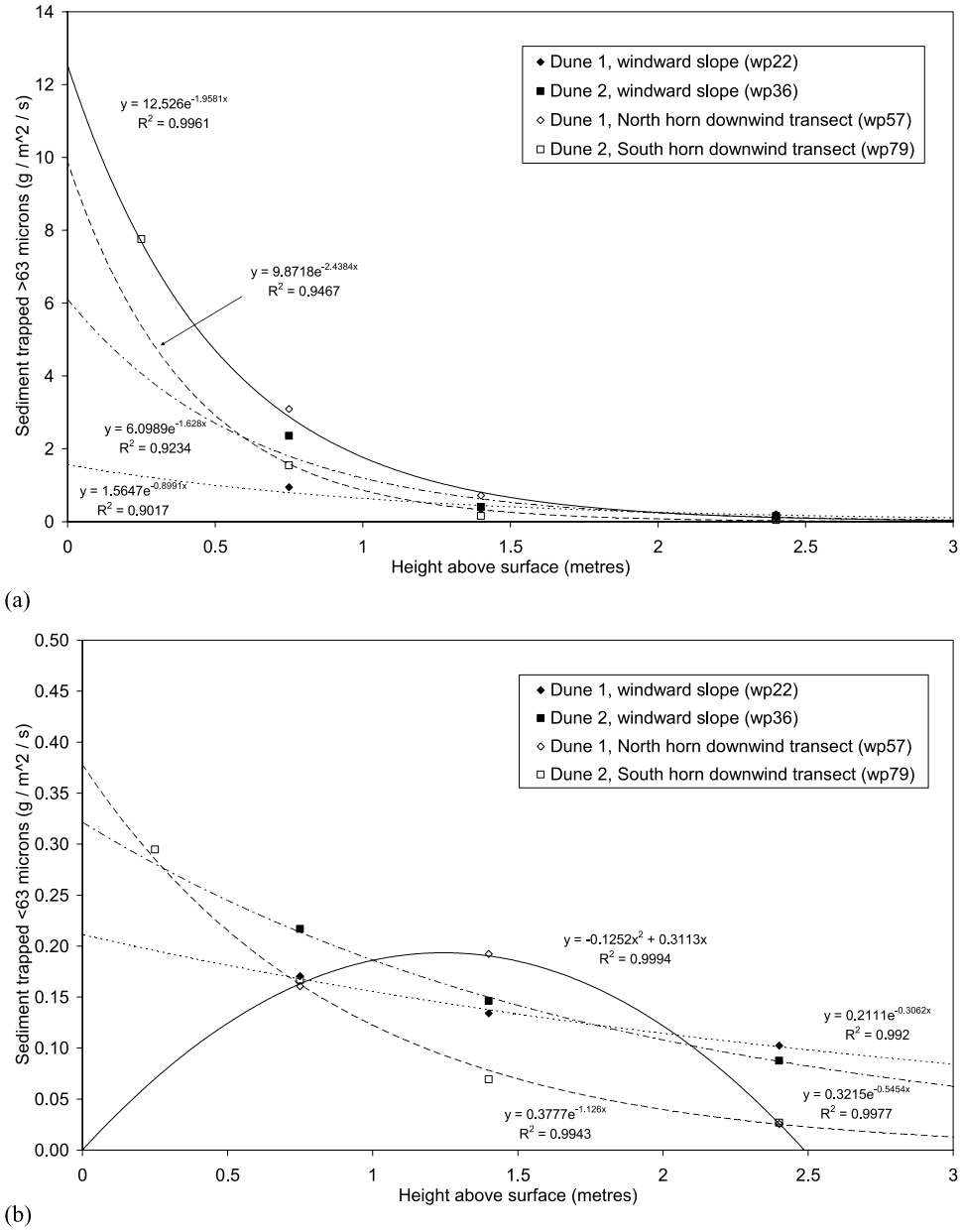

Figure 5. Horizontal sediment flux density of (a) the saltating fraction (>63 μm) and (b) the coarse dust fraction (<63 μm) measured at several heights above the surface for selected locations in the study area. The measurements are fitted with exponential and polynomial functions where appropriate.

diatomite flakes sitting on the surface; (6) angular diatomite derived from the surface itself; (7) pea gravel; (8) and large quartzose gravel. The classified samples were located on a map of the study area and used to identify broad patterns in the variation of surface types.

3. Results

3.1. Horizontal Sediment Density Flux Profiles and Integrated Flux

[18] Examples of the horizontal flux density of the saltation fraction (>63 μm) at several heights and for locations on the windward slope and downwind transects of Dunes 1 and 2 are shown in Figure 5a (Dune 3 is excluded for the reasons given below). The flux densities fit well with exponential profiles in all these cases. A justification for conducting the sediment horizontal flux integration to the surface is provided by a measurement in the saltation layer at 0.25 m above the surface (on Dune 2, southern horn, downwind transect). Examples of the coarse dust fraction (<63 μm) for the same heights and at the same locations as those of the saltation fraction, are shown in Figure 5b. An exponential profile is also a good fit for the coarse horizontal dust flux density profiles and the extrapolation of the integration to the surface is justified using the flux measurement at 0.25 m. As expected, the amount of coarse dust near the surface is small and the decline with height is much less than that of the saltation fraction. The exception to this pattern occurs for the site wp57 (Figure 5b)

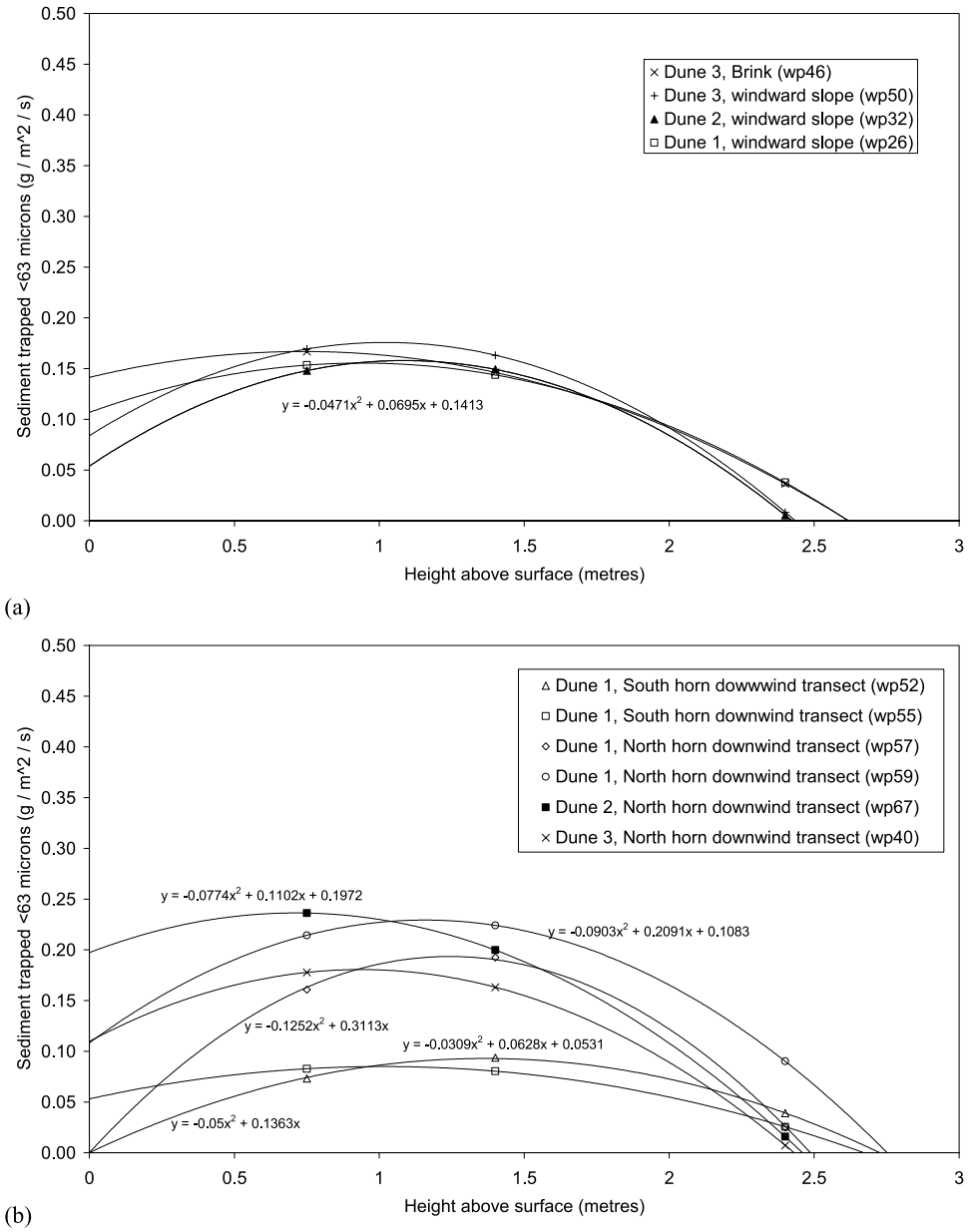

Figure 6. Horizontal sediment flux density of the coarse dust fraction (<63 μm) measured at several heights above the surface at locations on the (a) windward slope and (b) the downwind transect of the mega-barchan dunes where the vertical profiles do not conform to the expected exponential or power functions. The measurements are fitted with polynomial functions.

on the northern horn downwind of Dune 1. The flux density profile of the coarse dust fraction at this site does not conform to an exponential profile i.e., there is a bulge or a kink in the profile at 1.4 m (Figure 5b). This kink is interpreted as a displacement upwards of the coarse dust fraction as a consequence of preferential heating of the surface despite turbulence [*Butler et al.*, 2005] due to mineral color variations heating the closest air and reduced connectivity caused by variation in surface roughness; there could be other explanations. A polynomial is used to fit these data based on that interpretation. Figure 6a shows other profiles of the coarse dust fraction that do not conform to the exponential function, all of which also come from sites on the windward slopes of dunes. The polynomial fits of the curves for these sites are very similar to each other and predict a small amount of the coarse dust fraction near the surface. In contrast, the coarse dust fraction profiles downwind of the dunes that do not conform to exponential profiles, are much more variable in their vertical pattern (Figure 6b).

[19] The horizontal flux densities of the saltation fraction and the coarse dust fraction were integrated separately between 0 m and 3 m above the surface at each location using exponential and polynomial functions as appropriate. Table 2 shows the integrated load for the saltation fraction (>63 μm), the coarse dust fraction (<63 μm) and the ratio of the load of the two fractions at each location. Summary statistics are shown in Table 3

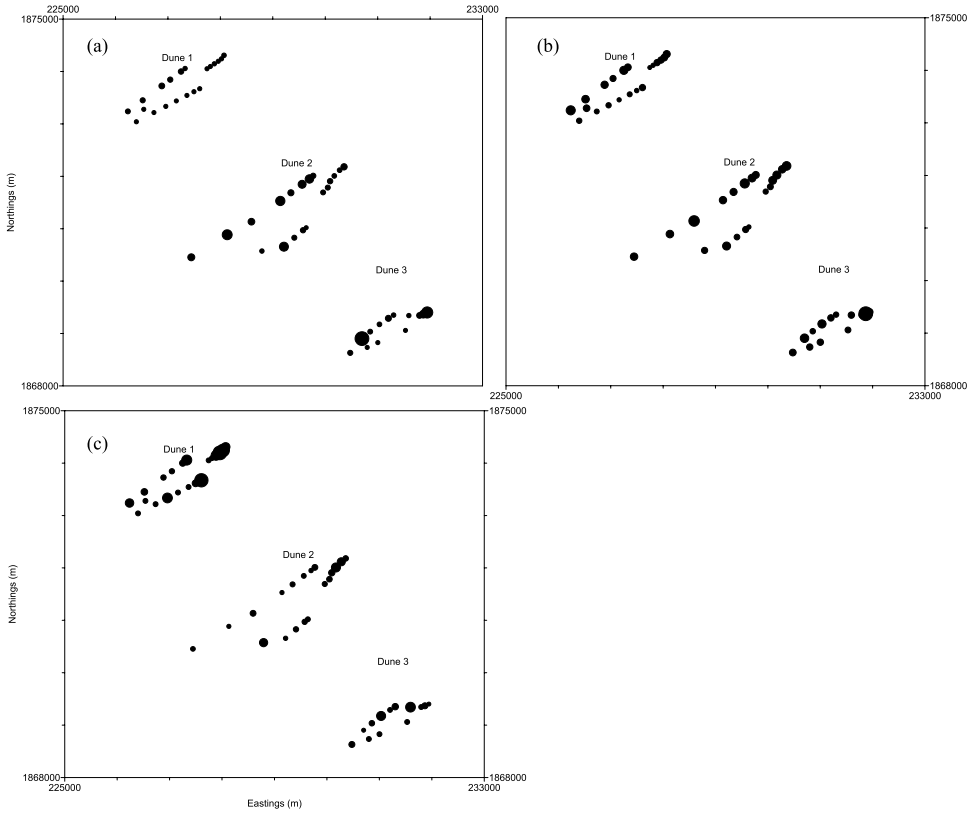

Figure 7. Location and magnitude (g m^{-1} s^{-1}) of integrated (0–3 m) horizontal sediment flux >63 μm (a) and that <63 μm (b) and relative ratio (c; see text for details). The symbols are linearly scaled between 0.002 and 0.4 g m^{-1} s^{-1} (a), 0.0004 and 0.01 g m^{-1} s^{-1} (b) and 0.01 and 0.27 (c).

for each dune region of the sampled area. A spatial representation of these data is given in Figure 7. The statistics show there to be a similar amount of coarse dust in each of the dune regions (upwind of the dune, windward slope of the dune, and downwind transects; Table 3; Figure 7b). There is a major exception to this generalization at the toe of Dune 3, which is the site where the largest amount of coarse dust was collected. The amount of the saltation fraction varies between dunes: the amount is smallest on Dune 1; Dunes 2 and 3 show larger and similar amounts (Table 3 and Figure 7b). These generalizations hide local variation within the samples obtained from the diatomite floor and the windward slopes of the dunes (see below).

[20] The ratio of saltation fraction to the coarse dust fraction is used to standardize for the variation in the saltation fraction and its influence on dust transport (Table 3). The relationship between the amount of material in saltation and the amount of coarse dust, standardized by the amount in the saltation fraction, is shown in Figure 8 where the predictive nature of the relationship is evident. The ratio is evident in Figure 7c and shows that, despite the small amounts of saltation fraction on Dune 1, there was proportionally twice as much coarse dust caught there than on Dunes 2 and 3 (Table 3). This distinction between Dune 1 and the other dunes is also evident in the clustering of symbols in Figure 8. The traps at some locations caught such small amounts of the saltation fraction that a misleading ratio occurred when the saltation fraction was divided by the amount of the coarse dust fraction. A threshold of 0.01 g m^{-1} s^{-1} in the saltation fraction was therefore used to identify those locations for which the ratio was not calculated and these were excluded in the summary statistics (Table 3) and in the ratio relationship (Figure 8).

3.2. Surface Type Classification

[21] The surface classification is shown in Figure 9. The study area is separated into two by the line drawn on the diagram. East of the line there is white diatomite either as a hard surface or fragments in accumulations on the surface (Classes 5 and 6, respectively). West of the line there are quartz mega-ripples, pea gravel and accumulations of large-sized gravel (Classes 3, 7 and 8 respectively). This division of the study area appears to follow the lighter and darker tones of Band 3 (near-infrared light) of the satellite imagery shown in the extract (Figure 1). The distribution of the dunes is independent of the surface type classification: they are found in both regions.

3.3. Particle Size Distribution of Surface and Trapped Sediment

[22] Particle size distributions (PSDs) were selected to represent the variation in the size of material moving over Dunes 1 and 2 (Figure 10). PSDs for Dune 3 were not used because the origin of the material in this dune is not evident, perhaps because of its proximity to the dividing line between the two groups in the surface-type classification. The PSDs are presented using the log-log distribution of

Table 2. Integrated (0–3 m) Horizontal Dust Flux for the Saltation Fraction (>63 μm), the Coarse Dust Fraction (<63 μm) and the Ratio for Both Fractions at Each Location[a]

Label, wp	Class	Location	Eastings, m	Northings, m	Crest Distance, m	Height, m	Saltation >63 μm ($g\ m^{-1}\ s^{-1}$)	Dust <63 μm ($g\ m^{-1}\ s^{-1}$)	Ratio
21	dune 1	upwind	228069	1874309	-412.93	171	0.0257	0.0034	0.1343
22	dune 1	toe	228022	1874243	-335.90	171	0.0134	0.0032	0.2370
23	dune 1	transect	227960	1874196	-258.21	175	0.0103	0.0028	0.2698
26	dune 1	transect	227885	1874147	-168.63	196	0.0160	0.0026	0.1634
24	dune 1	transect	227809	1874096	-77.10	209	0.0079	0.0007	-
25	dune 1	crest	227745	1874053	0.00	219	0.0087	0.0004	-
27	dune 1	north horn	227327	1874058	418.03	190	0.0184	0.0032	0.1717
28	floor 1	transect	227250	1874000	497.83	192	0.0618	0.0045	0.0721
57	floor 1	transect	227044	1873845	731.21	177	0.0549	0.0025	0.0460
58	floor 1	transect	226883	1873725	922.29	176	0.0748	0.0036	0.0487
59	floor 1	transect	226519	1873451	1365.83	176	0.0484	0.0039	0.0810
82	floor 1	transect	226539	1873279	1433.01	173	0.0092	0.0030	-
60	floor 1	transect	226236	1873239	1714.55	174	0.0416	0.0054	0.1293
29	dune 1	south horn	227606	1873672	405.56	196	0.0104	0.0027	0.2576
30	floor 1	transect	227496	1873615	503.83	195	0.0109	0.0009	0.0863
52	floor 1	transect	227362	1873544	637.00	177	0.0081	0.0014	-
53	floor 1	transect	227160	1873439	848.07	177	0.0051	0.0007	-
54	floor 1	transect	226959	1873335	1064.58	178	0.0106	0.0018	0.1660
55	floor 1	transect	226733	1873217	1312.65	177	0.0069	0.0013	-
56	floor 1	transect	226398	1873041	1684.80	178	0.0078	0.0019	-
35	dune 2	upwind	230358	1872181	-630.35	162	0.0967	0.0049	0.0510
36	dune 2	toe	230274	1872117	-528.21	163	0.0318	0.0038	0.1191
34	dune 2	transect	230172	1872008	-380.26	205	0.0301	0.0044	0.1455
33	dune 2	transect	230092	1871907	-251.96	221	0.0578	0.0042	0.0727
32	dune 2	transect	230048	1871785	-128.00	225	0.0435	0.0024	0.0546
31	dune 2	crest	229959	1871693	0.00	231	0.0402	0.0016	0.0405
63	dune 2	north horn	229770	1872010	369.07	153	0.0550	0.0033	0.0606
64	floor 2	transect	229698	1871950	366.29	152	0.1825	0.0041	0.0226
65	floor 2	transect	229559	1871848	428.98	150	0.1626	0.0055	0.0336
66	floor 2	transect	229345	1871686	614.04	151	0.0878	0.0035	0.0397
67	floor 2	transect	229143	1871530	832.12	150	0.2151	0.0038	0.0174
68	floor 2	transect	228592	1871134	1476.88	156	0.1119	0.0068	0.0605
80	floor 2	transect	228130	1870885	1999.53	178	0.2424	0.0040	0.0163
81	floor 2	transect	227445	1870455	2802.29	180	0.1229	0.0038	0.0308
37	dune 2	south horn	229637	1871020	746.07	149	0.0018	0.0008	-
38	floor 2	transect	229576	1870971	817.30	150	0.0554	0.0025	0.0458
69	floor 2	transect	229410	1870828	1024.51	165	0.0451	0.0021	0.0466
70	floor 2	transect	229212	1870657	1277.23	153	0.2044	0.0044	0.0214
79	floor 2	transect	228792	1870574	1616.80	174	0.0214	0.0026	0.1228
45	dune 3	upwind	231944	1869402	-354.94	158	0.2906	0.0031	0.0107
51	dune 3	toe	231869	1869369	-276.23	168	0.1526	0.0099	0.0649
50	dune 3	transect	231798	1869345	-204.01	170	0.0748	0.0027	0.0362
46	dune 3	brink 1	231594	1869343	0.00	190	0.0172	0.0028	0.1636
42	dune 3	north horn	231303	1869352	291.14	155	0.0233	0.0018	0.0759
40	floor 3	transect	231204	1869290	393.58	150	0.0846	0.0028	0.0333
71	floor 3	transect	231033	1869175	585.62	157	0.0312	0.0045	0.1453
72	floor 3	transect	230857	1869036	798.38	159	0.0374	0.0019	0.0512
73	floor 3	transect	230700	1868903	996.41	167	0.3970	0.0048	0.0121
74	floor 3	transect	230476	1868631	1325.47	165	0.0489	0.0032	0.0644
44	floor 3	transect	231530	1869060	290.15	153	0.0064	0.0023	-
76	floor 3	transect	231002	1868827	785.32	172	0.0083	0.0028	-
77	floor 3	transect	230800	1868735	1000.05	174	0.0071	0.0028	-

[a](-) In cells indicates that the ratio has not been calculated because the small amounts of saltation fraction at that location produce misleading values for the ratio.

Bagnold [1941] to enable the small volumes of small diameter size fractions to be examined (Figure 10). A threshold of 0.1% volume is used to truncate the display of the PSDs.

[23] All the surface samples from the dunes show modal size diameters at around 200 μm and 800 μm. At 0.75 m above the surface of Dune 1 the PSD shows proportions of material with similar proportions in modal size diameters around 3 μm, 17 μm and an increased proportion in that around 140 μm (Figure 10a). Similar modal size diameters are evident at 1.4 m above the surface, but they contain a larger proportion of material than that found at 0.75 m. The coarsest size mode evident in the surface sample at this site (1000 μm) is also present at 0.75 m height, but it is not present in the higher traps. The smallest size modes are not present in the highest trap (2.4 m) contrary to expectations. The reason for this is unclear although local conditions may be responsible. At 0.75 m above the surface of Dune 2 there is a mode around 800 μm that has a similar proportion of material to that found at around 200 μm (Figure 10b). In contrast to Dune 1, there is a 1000 μm mode at 1.4 m above the surface of Dune 2, but this mode is not evident at 2.4 m

Table 3. Summary Statistics of the Sampled 'Dune' Regions, on and Around Each Dune, for Integrated (0–3 m) Horizontal Dust Flux for the Saltation Fraction (>63 μm), the Coarse Dust Fraction (<63 μm) and the Ratio for Both Fractions at Each Location

	'Dune' 1			'Dune' 2			'Dune' 3		
	>63 μm (g m^{-1} s^{-1})	<63 μm (g m^{-1} s^{-1})	Ratio	>63 μm (g m^{-1} s^{-1})	<63 μm (g m^{-1} s^{-1})	Ratio	>63 μm (g m^{-1} s^{-1})	<63 μm (g m^{-1} s^{-1})	Ratio
Minimum	0.0051	0.0004	0.0460	0.0018	0.0008	0.0163	0.0064	0.0018	0.0107
Maximum	0.0748	0.0054	0.2698	0.2424	0.0068	0.1455	0.3970	0.0099	0.1636
Median	0.0107	0.0026	0.1343	0.0578	0.0038	0.0462	0.0374	0.0028	0.0578
Average	0.0430	0.0037	0.1058	0.1211	0.0036	0.0416	0.0776	0.0031	0.0613
Std	0.0250	0.0010	0.0802	0.0806	0.0016	0.0303	0.1318	0.0010	0.0509

above the surface as on Dune 1. There appears to be an upwards fining of the smallest modal size diameters (2 μm, 4 μm and 6 μm) and an increase in the proportion of these modes above the surface of Dune 2 (Figure 10b). The PSDs of material in saltation at 0.25 m above the surface and downwind of Dune 2 are similar to the size of material found at the surface of Dunes 1 and 2 (Figure 11). However, the size of saltating material immediately downwind of Dune 1 has fine size modes (2 μm, 12 μm and 80 μm), which are not usually present in the saltation layer of dune material.

4. Discussion

4.1. Spatial Variation in Erodibility and its Relationship With the Magnitude of Horizontal Dust Flux

[24] There is a simple east-west division of surface type in the study area (Figure 9), a division that is also evident on the satellite imagery (Figure 1). Given the very small contribution of soil moisture and vegetation that might otherwise contribute to the reflectance in Band 3, the darker tones on Figure 1 are associated with low reflectance (large absorption), which is typical of the presence of iron oxides [e.g., haematite, goethite etc.; *Stoner and Baumgardner*, 1981]. Thus the western portion of the study area is broadly covered by 'iron-oxide-rich' material, which is found in mega-ripples and polished gravel of varying sizes, which have coatings of desert varnish. The lighter tones in the eastern part of the study area are likely therefore to indicate the absence of those oxides (large reflectance) and are typical of the off-white color of the massive diatomite, on which there are some accumulations of abraded diatomite flakes. All the dune surfaces are more similar in their reflectance to the western iron-oxide surface group of classes than to the eastern iron-light group (Figure 1). The sharp contrast between the leading and trailing edges of the dunes and the background on which they travel probably indicates that their surfaces comprise a mixture of particles of iron-oxide-coated quartz and of diatomite. Dune 1 is contained within the westerly 'iron-oxide' group of classes and appears to have more of the iron-oxide-coated quartz than Dunes 2 and 3, which are located in the easterly 'diatomite' group of classes. The two-part grouping of surface types may thus provide a basis for an explanation of dust emission (see section 4.2). Further, it suggests that global-scale dust emission models that use surface reflectance as a simple approximation of variation in source strength require modification to account for the preferential erodibility of light surfaces in contrast to dark surfaces.

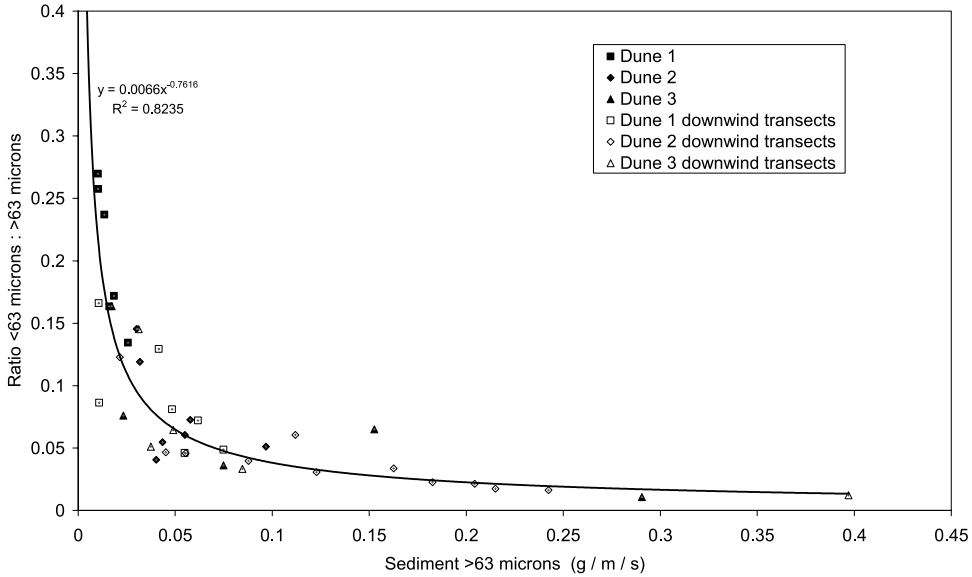

Figure 8. Relationship between the saltation fraction and the coarse dust fraction (standardized by the saltation fraction) for each dune and each downwind transect. A power model is fitted to all data excluding those pairs that are associated with amounts of the saltation fraction less than 0.01 g m^{-1} s^{-1}.

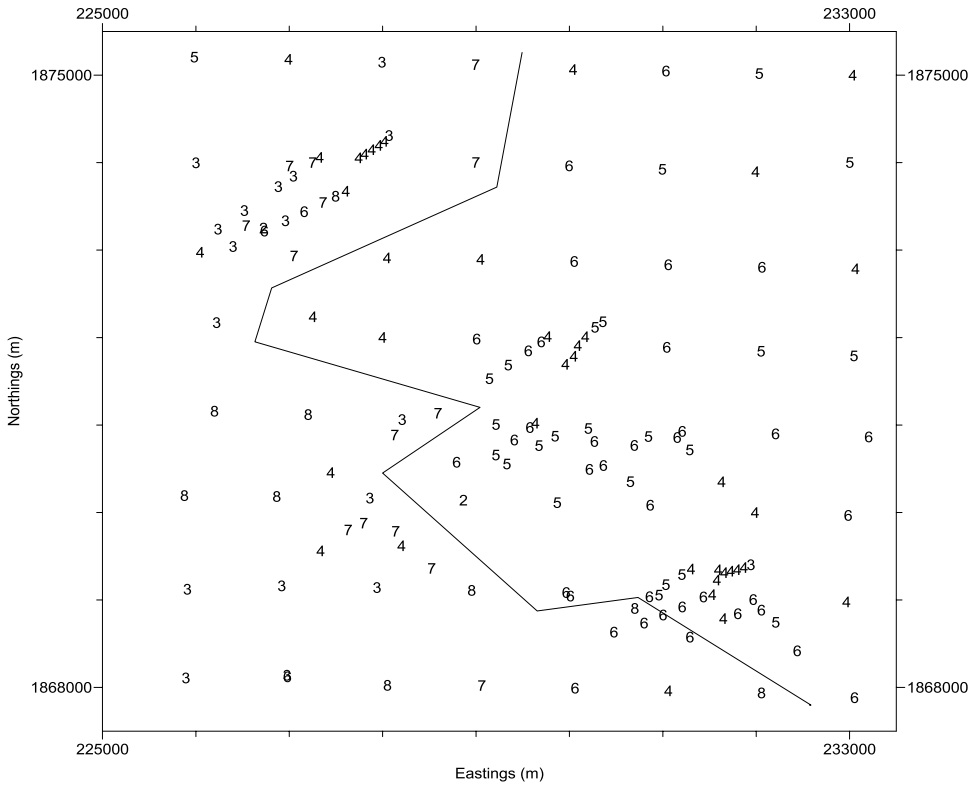

Figure 9. Map of the study area showing the locations of surface samples classified according to surface type: (3) mega-ripple material, (4) dune material containing diatomite flakes, (5) rounded/abraded diatomite flakes sitting on the surface. (6) angular diatomite derived from the surface itself, (7), pea gravel, (8) and large gravel. The line divides the study area into an area associated with diatomite (east) and the other with iron-oxide-coated material (west) and closely matches the satellite imagery of the study area.

[25] All profiles containing 'kinks' in the vertical profiles of dust caught downwind of the dunes (Figure 6), were in the 'iron-oxide' surface-type (Figure 6b). 'Kinks' in dust profiles are believed to be caused by heating of the surface, which despite turbulence, lifts air and suspended dust to heights not typically associated with an exponential, dust profile [*Butler et al.*, 2005]. The occurrence of 'kinky' vertical dust profiles above red-colored iron-oxide surfaces is consistent with the preferential absorption of radiation by the darker-colored minerals. However, this explanation is unlikely fully to explain 'kinky' profiles on the dunes (Figure 6a). It may be that the heating rate is also modulated by the roughness of the surface of the dunes. The second indication of the importance of the surface type for dust transport is the finding that the largest average amount of the standardized coarse dust fraction occurs on Dune 1 (Figures 7 and 8 and Table 3). In other words, for the same amount of the saltation fraction moving over the dunes, more dust is produced on Dune 1 than on Dunes 2 or 3. This more efficient production of dust on Dune 1 could mean (a) that dust is being released from an available store in the surface of the dune or (b) by abrasion. On Dunes 2 and 3, dust is apparently produced by bombardment by a saltation fraction, which is greater than on Dune 1. Thus dust appears to be produced differently in the western region dominated by iron-oxide-coated quartz and gravel, than in the eastern region dominated by diatomite.

4.2. Dust Production Processes Elucidated Using the Particle Size of Horizontal Dust Flux

[26] The suggestion (above) that dunes are stores of dust is refuted by the data on particle size distributions of surface samples on the windward slopes of Dunes 1 and 2 (Figure 10). The PSDs of all the dune surfaces are bimodal, very similar to each other and show no evidence of material any finer than about 70 μm. This finding is to be expected in a highly dynamic dune environment in which the surface is constantly being remobilized by the impact of saltating particles, which must winnow out fine material. An argument that difference in efficiency of dust production between the dunes comes from differences in wind erosivity caused by differences in wind velocity or 'speed-up' over different dunes is hard to sustain because the gradients of dune windward slopes are very similar. A better argument is that the more efficient dust production around Dune 1 than around the other dunes is because the saltators are themselves abraded when they are driven by bombardment against the tough, durable iron-oxide-coated quartz and gravel surface of the western region. This might happen immediately downwind of the barchan dune horns (Figures 7 and 9) where the saltating material is transferred from the soft, yielding dune surface to the hard unyielding gravel surface. Evidence to support this argument is provided by the PSDs of material in the saltation layer (0.25 m above the surface; Figure 11). The PSD of

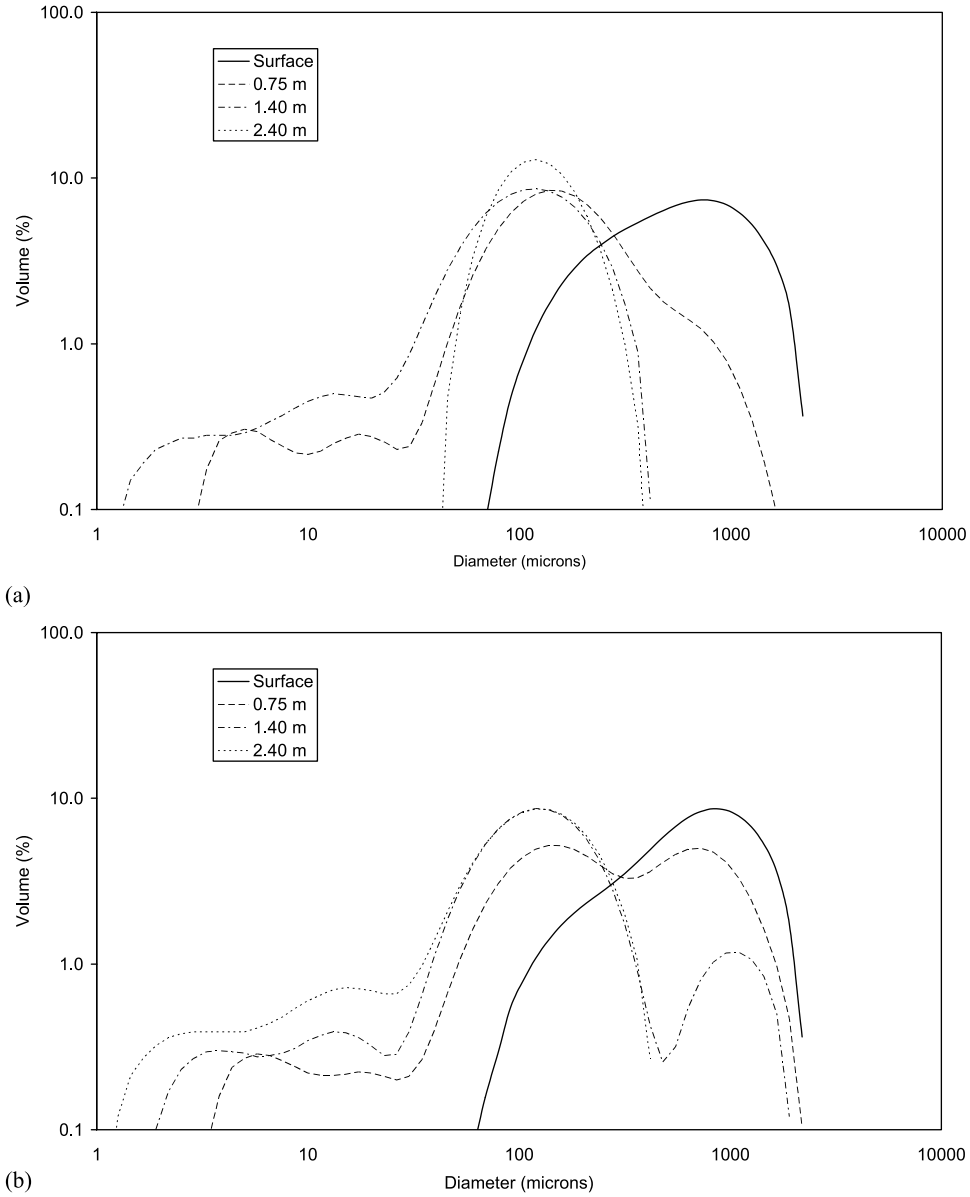

Figure 10. Particle size distributions of an unconsolidated surface sample and sediment trapped at three heights above the surface (0.75 m, 1.4 m, and 2.4 m) on the central portion of the windward slope of dune 1 (a) and dune 2 (b). Note the logarithmic scale on both axes.

material moving over the gravel surface downwind of Dune 1 shows size modes at around 2 μm, 12 μm and 80 μm. The presence of such quantities of fine material in the saltation layers at these sites suggests that large quantities of dust are produced on the western, more-quartzose surface type and also that the mechanism of dust production in this region is associated with the breakdown of the saltating material, as suggested with less evidence by *Warren et al.* [2007] in a process similar to the abrasion of (soil) aggregates at the surface of agricultural fields [*Gomes et al.*, 1990; *Shao and Raupach*, 1993; *Alfaro et al.*, 1997]. Such size modes are absent from the saltation layer on Dunes 2 and 3 (eastern "diatomite" region), where the saltation layer is dominated by size modes around 100 μm and 800 μm (Figure 11), which implies that the diatomite fragments have not been broken into small pieces during abrasion in this area.

[27] The hypothesis that prolific dust production occurs when saltating material breaks down on a hard surface cannot explain the occurrence of large standardized coarse dust fractions on the windward slope of Dune 1 (Figures 7 and 8 and Table 3). The surface on all three dunes is soft and yielding to the impact of saltators of all kinds. There is no difference in the size of material at the surface of Dunes 1 and 2 (Figure 10) and there is no difference between the sizes of material saltating at these sites (Figure 11). The only other major difference in surface material between Dunes 1 and 2 is that there is a larger proportion of iron-oxide-coated quartz on the surface of Dune 1 than on Dune 2 (Figure 1). For the same size of

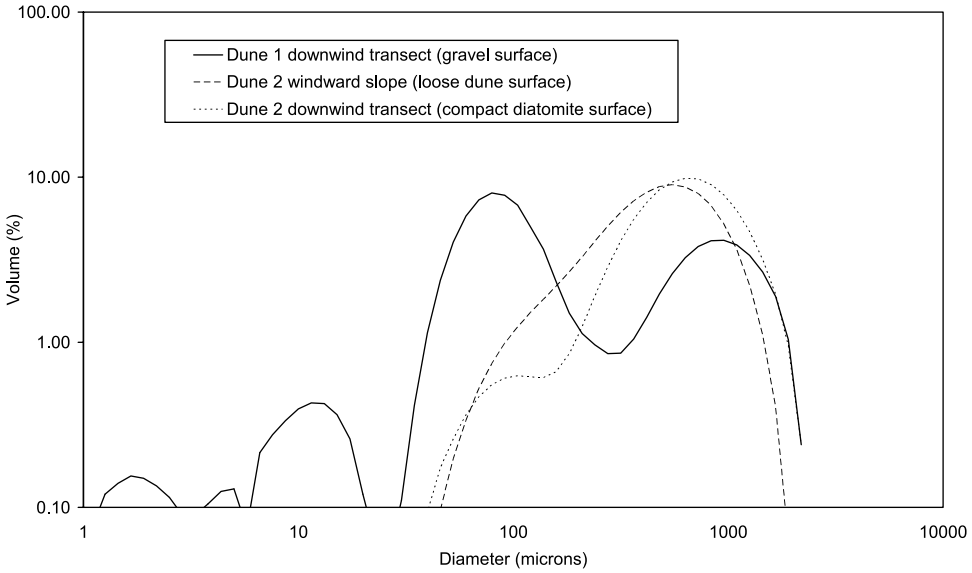

Figure 11. Particle size distributions of sediment trapped at 0.25 m above the surface of the windward slope and the downwind transect of dunes 1 and 2. Note the logarithmic scale on both axes.

material, iron-oxide-coated quartz is much heavier [density of quartz is 2.6–2.65g cm^{-3}; *Tanaka et al.*, 2001] than diatomite, whose density by our estimate (based on a straightforward volume displacement experiment), is 0.9 g cm^{-3} (nearly three times less than for quartz). The most likely explanation for the efficient production of dust on the windward slope of Dune 1 is abrasion of the diatomite flakes by bombardment of the surface and during mid-air collisions by the greater momentum transfer of a larger proportion of iron-oxide-coated quartz sand. The corollary to this argument is that where there is only a small proportion of iron-oxide-coated quartz sand (as on Dune 2), most collisions are between diatomite fragments, in which case the coarse size mode of diatomitic fragments should be preserved. Thus the hypothesis is that a mixed mineralogy of saltators influences the size of dust emission. Evidence to support this hypothesis is contained in the difference between the PSDs at 0.75 m on the windward slopes of Dune 1 and 2 (Figure 10). There is only a small amount of the coarsest (1000 μm) size mode of diatomitic fragments at 0.75 m above the surface of Dune 1, but a substantial amount of that mode at the same height on Dune 2. Furthermore, the presence of material in that mode at 1.4 m above the surface of Dune 2 (Figure 10b) is indicative of the small density and aerodynamic shape of the diatomitic fragments.

4.3. Implications for Large Area Dust Emission Modeling and Radiative Properties of the Atmosphere

[28] A straightforward explanation for the prolific production of dust from the Bodélé is its production in flow over and around the barchan dunes: regarding the dunes as ''dust mills'' [*Warren et al.*, 2007]. Dust can be produced even at wind shear values below the threshold of movement on the diatomite floor, because of the increase in wind shear up (and around) the dunes, which cause the abrasion of heterogeneous mixtures of sizes and types of particles on the dunes and inject the dust formed in this way into the atmosphere at the dune crests, which are up to 70 m above the diatomite floor. This hypothesis is consistent with observations of frequent 'smoking' at the crests of the mega-barchans, even at low wind shear measured at the upwind toe of the dune. Furthermore, the results presented above suggest that speed-up and low-turbulent flow on the windward slope increases the generation of dust, not only as a product of increased sediment transport, but also as a function of the mineralogy of the saltators. These ideas have considerable implications for the type and size of dust emission from the Bodélé and the atmospheric layers in which it is distributed, mixed and allowed to deposit [*Tegen et al.*, 2006].

[29] The model of dust production in the Bodélé of *Tegen et al.* [2006] used a horizontal resolution of 7 km, which is approximately the same as the size of the study area described here. The model assumes that roughness and soil texture are constant within this grid cell. Our measurements show that there is considerable heterogeneity within one such cell. We do not yet know if the same degree of surface heterogeneity occurs in other similarly sized cells across the Bodélé Depression. In the Tegen model the 'soils' in the Bodélé Depression were assumed to consist of uniformly textured particles with modal diameters of 15 μm, which disaggregated into 2 μm dust particles during saltation events [*Tegen et al.*, 2006, p. 4347]. Our measurements show that the surface materials are not typical soils and that the size-distributions of the dune material are bi-modal with typical modal diameters around 200 μm and 800 μm. The saltating material in transport upwind, across and downwind of the dunes has coarse modes similar to those of the surface material as well as fine modal diameters of around 3 μm, 17 μm, and 140 μm. We have provided some evidence to suggest that these fine fractions are associated with the sizes of individual diatoms. There also appears to be an upwards fining of the modal size diameters (2 μm, 4 μm and 6 μm) in transport above the surface of the dunes. The finding of multiple modes is consistent with saltation/abrasion/sandblasting theory and a time-varying dust size

distribution which is dependent on erodibility and erosivity [*Alfaro and Gomes*, 2001; *Grini and Zender*, 2004]. It contrasts with the retrievals of size distributions from Sun photometer measurements made in the study area [*Todd et al.*, 2007], which provided a single particle radius at 2 μm, a size that is comparable to estimates for other desert dust. The results presented here and elsewhere [*Warren et al.*, 2007] suggest that the mechanisms and the nature of the dust produced in the Bodélé Depression are unusual, perhaps globally unique. This finding is significant because the model of *Tegen et al.* [2006] was validated, in the absence of direct measurements of emission, against dust optical thicknesses (DOTs) based on the retrieved size distribution. There is a major discrepancy between the modal size measurements presented here and the retrieved size distribution of *Todd et al.* [2007]. The sun and sky radiance measurements were made up to ca. 70 m beneath a dust 'canopy' of heterogeneous mineralogy and size (up to 1000 μm) and abundance that caused a reduction in light and temperature. Under these conditions straight-forward relationships between light extinction and particle size may not hold and assumptions about homogeneity in size and vertical variation throughout the boundary layer [*Dubovik and King*, 2000] appear likely to retrieve size distributions that are unrealistic.

[30] The model of *Tegen et al.* [2006] also assumed that the mass of dust produced in the Bodélé was directly proportional to the mass of the saltators. This assumption appears to be reasonable at locations in the study area where the saltators are dominantly particles of one material, such as diatomite (as on Dune 2). However, at many locations in the study area the saltators are mixtures of quartz sand and diatomite flakes (as on Dune 1). The spatial variation in the mass and density of abraders may have an important effect on dust emission estimates derived from models. If, as suggested here, heterogeneity in surface types, mineralogy of saltators and particle sizes are important in dust production, better estimates of dust production would come from mapping the surface types, the size and location of dunes, and the locations of zones of incursion of quartz sand. Furthermore, we have shown that the mixture of the saltators and the surface that they impact is important to the magnitude and particle size of dust they produce. There is evidently a need to account for these features in dust emission modeling over large areas, not least because of the apparently distinct mechanisms by which dust is produced in each region.

5. Conclusions

[31] The work presented here provides the first ground-based measurements of the spatial and vertical variation in horizontal dust flux magnitude and particle size from the Earth's largest source. Comparisons have been made here between the results obtained from the ground-based measurements and those mechanisms of emission assumed in current dust models to characterize the processes of dust production over large areas and in particular the Bodélé. The comparison suggests that the following aspects of dust emission modeling of the Bodélé may require modification to provide more precise and accurate estimates of the magnitude of dust and radiation fluxes:

[32] Dust production is spatially inhomogeneous because of the distribution of mega-barchan dunes and of different types of surface in the inter-dune areas. Surfaces with mixtures of iron-oxide-coated quartz and diatomite may have different effects on the efficiency of dust production, because of their different erodibility (compactness, surface type, availability of loose erodible material etc.). Topographic speed-up over the dunes suggests that separate thresholds for dust emission are required on the playa surface and on the dunes. The extent of the significance of this effect could not be tested with the measurements available in this study.

[33] Emissions of dust from the Bodélé do not consist of one modal size at 2 μm (as used in some large area dust emission models), but many modes with diameters between 2 μm and 50 μm. Smaller modal sizes could not be detected with the methods used here. The different modal sizes appear to be associated with the size of the diatom species and their disintegration during saltation. Since the density of the diatomite (0.9 g cm^{-3}) in the Bodélé Depression is almost three times less than the density of quartz, the typical modeled size of dust emission (10 μm size) may have to be extended to account for the unusual aerodynamic properties of dispersed material.

[34] Heterogeneous sizes (up to 1000 μm) and mineralogies of particles are injected into the atmosphere at up to 70 m above the playa surface, even at below-threshold wind shears on the diatomite surface. The majority of these injected particles will almost certainly sink down again. Measurements of sun and sky radiance beneath and/or among this dust 'canopy' retrieved size distributions that did not match dust size measurements. Sparse ground-based measurements are unlikely to represent the spatial variations in dust production processes described here. Upscaling assumptions of homogeneous erodibility (e.g., roughness, soil type, dust size) for regional dust emission modeling may be considerably improved with geomorphic information on dunes and surface type.

[35] These considerations suggest three topics for further research, the results of which may define the exact nature of the parameters required for improvements in emission modeling:

[36] The biggest gap in knowledge of dust from the Bodélé concerns the vertical dust flux. Experiments should be designed to isolate the effect of the material properties on dust production and its vertical flux. This could involve a dust production machine using the various mixtures of surface material in the study area. A wind-tunnel experiment could isolate the effects on the amount of dust production and its particle size over different types of surface under bombardment by homogeneous and mixtures of abrader types. In the present study a strong relationship was established between the saltation fraction (>63 μm) and the coarse dust fraction (<63 μm) standardized according to the variation in the amount of the saltation fraction at each location. It is based on similar relationship established in the literature [*Gillette et al.*, 1997] and may prove useful in extending dust production estimates across the study area and the entire Bodélé.

[37] This paper shows considerable variation in the magnitude of horizontal dust flux and its particle size within a 7 km $\times$ 8 km area. This area is similar to the size of homogeneous cells used in regional dust emission models.

It is unclear whether the actual variation within that grid cell is important for precise dust emission estimates. There appears to be a need for statistical upscaling of the samples perhaps using geostatistical spatial uncertainty. There is also a need for the development of a finer-resolution model of horizontal dust flux that incorporates variation according to position relative to the distribution of mega-barchan dunes and the surface on which they sit. This type of model could make use of fine resolution satellite imagery (e.g., Landsat ETM or SPOT) or digital elevation data to classify the area in such a way as to produce dust emission estimates for the dunes and their surrounding surface types.

[38] Dust samples from the Bodélé passed through a laser sizer may be used to measure the angular reflectance for a narrow range of wave bands. This type of measurement could be used to retrieve the values of radiative transfer model parameters and to investigate the variation in those parameters across space and above the surface (diatomite floor and dune crests).

[39] **Acknowledgments.** AC, AW and CB are grateful to the Royal Geographical Society and the Gilchrist Educational Trust for funding to undertake the field phase of this research. AW is indebted to the Dean's Fund and the Department of Geography at University College London. We are grateful to David Ryves for assisting with the diatom identification and to Ronald L. Miller and an anonymous referee for incisive and constructive comments. Any omissions or inaccuracies in the paper remain the sole responsibility of the authors.

References

Alfaro, S. C., and L. Gomes (2001), Modeling mineral aerosol production by wind erosion: Emission intensities and aerosol size distributions in source areas, *J. Geophys. Res.-Atmos.*, *106*(D16), 18,075–18,084.

Alfaro, S. C., A. Gaudichet, L. Gomes, and M. Maille' (1997), Modeling the size distribution of a soil aerosol produced by sandblasting, *J. Geophys. Res.*, *102*(D10), 11,239–11,249.

Bagnold, R. A. (1941), *The physics of blown sand and desert dunes*, Methuen, London, 265 pp. [2nd printing, 1954, 3rd printing 1960].

Bristow, C. S., N. Drake, and S. Armitage (2008), Deflation in the dustiest place on Earth: the Bodélé Depression, Chad, *Geomorphology*, in press.

Bullard, J. E., G. H. McTainsh, and C. Pudmenzky (2004), Aeolian abrasion and modes of fine particle production from natural red dune sands: an experimental study, *Sedimentology*, *51*(5), 1103–1125.

Butler, H. J., G. H McTainsh, W. L. Hogarth, and J. F. Leys (2005), Kinky profiles: Effects of soil surface heating upon vertical dust concentration profiles in the Channel Country of western Queensland, Australia, *J. Geophys. Res.*, *110*, F04025, doi:10.1029/2004JF000272.

Chappell, A. (1998), Dispersing sandy soil for measuring particle size distributions, *Catena*, *31*(4), 271–283.

Chappell, A., G. McTainsh, J. Leys, and C. Strong (2003a), Using geostatistics to elucidate temporal change in the spatial variation of aeolian sediment transport, *Earth Surf. Processes Landforms*, *28*, 567–585.

Chappell, A., G. McTainsh, J. Leys, and C. Strong (2003b), Simulations to optimise sampling of aeolian sediment transport for mapping in space and time, *Earth Surf. Processes Landforms*, *28*, 1223–1241.

Dong, Z. B., G. Q. Qian, W. Y. Luo, and H. T. Wang (2006), Analysis of the mass flux profiles of an aeolian saltating cloud, *J. Geophys. Res. Atmos.*, *111*(D16), art. no. D16111.

Drake, N., and C. S. Bristow (2006), Shorelines in the Sahara: Geomorphological evidence for an enhanced monsoon from palaeolake Megachad, *Holocene*, *16*(6), 901–911.

Dubovik, O., and M. D. King (2000), A flexible inversion algorithm for retrieval of aerosol optical properties from Sun and sky radiance measurements, *J. Geophys. Res.*, *105*(D16), 20,673–20,696.

Gillette, D. A. (1974), On the production of soil wind erosion aerosols having the potential for long range transport, *J. Rech. Atmos.*, *8*(3-4), 735–744.

Gillette, D. A. (1977), Fine particle emissions due to wind erosion, *Trans. Am. Soc. Agric. Eng.*, *20*(5), 890–897.

Gillette, D. A., D. W. Fryrear, T. E. Gill, T. Ley, T. A. Cahill, and E. A. Gearhart (1997), Relation of vertical flux of particles smaller than 10 (m to total aeolian horizontal mass flux at Owens Lake, *J. Geophys. Res. Atmos.*, *102*(D22), 26,009–26,016.

Ginoux, P., M. Chin, I. Tegen, J. Prospero, B. Holben, O. Dubovik, and S.-J. Lin (2001), Sources and distributions of dust aerosols simulated with the GOCART model, *J. Geophys. Res.*, *106*, 20,555–20,273.

Gomes, L., G. Bergametti, G. Coudé-Gaussan, and P. Rognon (1990), Submicron desert dusts: A sandblasting process, *J. Geophys. Res.*, *95*, 13,927–13,935.

Goossens, D., and Z. Offer (2000), Wind tunnel and field calibration of six aeolian dust samplers, *Atmos. Environ.*, *34*, 1043–1057.

Grini, A., and C. S. Zender (2004), Roles of saltation, sandblasting, and wind speed variability on mineral dust aerosol size distribution during the Puerto Rican Dust Experiment (PRIDE), *J. Geophys. Res.*, *109*(D7), D07202, doi:10.1029/2003JD004233.

Kuntze, H., R. Beinhauer, and G. Tetzlaff (1989), Quantifizierung der Bodenerosion durch Wind, *Mitt. Deutsch. Boden. Gesell.*, *59*(2), 1089–1094.

Lu, H., and Y. Shao (2001), Toward quantitative prediction of dust storms: An integrated wind erosion modelling system and its applications, *Environ. Modell. Softw.*, *16*(3), 233–249.

Mahowald, N., R. G. Bryant, J. del Corral, and L. Steinburger (2003), Ephemeral lakes and desert dust sources, *Geophys. Res. Lett.*, *30*(2), 1074–1078, 1074, doi:10.1029/2002GL016041.

Malvern Instruments (2003), *Operators guide*. Manual MAN0247 Issue 2.0. Malvern Instruments Ltd. Worcestershire.

Marticorena, B., G. Bergametti, B. Aumont, Y. Callot, C. N'Doume, and M. Legrand (1997), Modeling the atmospheric dust cycle: 2. Simulation of Saharan dust sources, *J. Geophys. Res. Atmos.*, *102*, 4387–4404.

Miller, R. L., R. V. Cakmur, Ja. Perlwitz, I. V. Geogdzhayev, P. Ginoux, K. E. Kohfeld, D. Koch, C. Prigent, R. Ruedy, G. A. Schmidt, and I. Tegen (2006), Mineral dust aerosols in the NASA Goddard Institute for Space Sciences ModelE atmospheric general circulation model, *J. Geophys. Res.*, *111*, D06208, doi:10.1029/2005JD005796.

Prospero, J. M., P. Ginoux, O. Torres, S. E. Nicholson, and T. E. Gill (2002), Environmental characterization of global sources of atmospheric soil dust identified with Total Ozone Mapping Spectrometer absorbing aerosol product, *Rev. Geophys.*, *40*(1), 1002, doi:10.1029/2000RG000095.

Shao, Y., and I. Lu (2000), A simple expression for wind erosion threshold friction velocity, *J. Geophys. Res.*, *105*, 22,437–22,443.

Shao, Y., and M. Raupach (1993), Effect of saltation bombardment by wind, *J. Geophys. Res*, *98*, 12,719–12,726.

Stoner, E. R., and M. F. Baumgardner (1981), Characteristic variations in reflectance of surface soils, *Soil Sci. Soc. Am. J.*, *45*, 1161–1165.

Stout, J. E., and T. M. Zobeck (1996), The Wolfforth field experiment. A wind erosion study, *Soil Sci.*, *161*(9), 616–632.

Tanaka, M., A. Mochizuki, T. Motomura, K. Shimura, M. Onishi, and Y. Okahata (2001), In situ studies on protein adsorption onto a poly(2-methoxyethylacrylate) surface by a quartz crystal microbalance, *Colloids Surfaces A: Physicochemical and Engineering Aspects*, *193*(1), 145–152.

Tegen, I., B. Heinold, M. C. Todd, J. Helmert, R. Washington, and O. Dubovik (2006), Modelling soil dust aerosol in the Bodélé Depression during the BoDEx campaign, *Atmos. Chem. Phys.*, *6*, 4345–4359.

Todd, M. C., R. Washington, J. V. Martins, O. Lizcano, G. M'Bainayel, and S. Engelstaedter (2007), Mineral dust emission from the Bodélé Depression, northern Chad during BoDEx 2005, *J. Geophys. Res.*, *112*(D6), D06207, doi:10.1029/2006JD007170.

Warren, A., A. Chappell, M. C. Todd, C. Bristow, N. Drake, S. Engelstaedter, V. Martins, S. M'bainayel, and R. Washington (2007), Dust-raising in the dustiest place on earth, *Geomorphology*, *92*(1-2), 25–37.

Washington, R., and M. C. Todd (2005), Atmospheric controls on mineral dust emission from the Bodélé Depression, Chad, *Geophys. Res. Lett.*, *32*(17), L17701, doi:10.1029/2005GL023597.

Washington, R., M. Todd, N. J. Middleton, and A. S. Goudie (2003), Dust-storm source areas determined by the total ozone monitoring spectrometer and surface observations, *Ann. Assoc. Am. Geographers*, *93*(2), 297–313.

Washington, R., M. C. Todd, S. Engelstaedter, S. Mbainayel, and F. Mitchel (2006), Dust and the low level circulation over the Bodélé Depression, Chad: Observations from BoDEx 2005, *J. Geophys. Res. Atmos.*, *111*(D3), Art. No. D03201.

Wilson, S. J., and R. U. Cooke (1980), *Wind erosion*, In: M. J. Kirkby, and M. J. Morgan (eds.) Soil Erosion, John Wiley and Sons, Chichester, pp. 217-251.

Zender, C. S., D. Newman, and O. Torres (2003), Spatial heterogeneity in aeolian erodibility: Uniform, topographic, geomorphic, and hydrologic hypotheses, *J. Geophys. Res.*, *108*(D17), 4543, doi:10.1029/2002JD003039.

Zobeck, T. M., G. Sterk, R. Funk, J.-L. Rajot, J. E. Stout, and R. S. Van Pelt (2003), Measurement and data analysis methods for field-scale wind erosion studies and model validation, *Earth Surf. Processes Landforms*, *28*(11), 1163–1188.

C. Bristow, School of Earth Sciences, Birkbeck College, University of London, Malet St, London WC1E 7HX, UK.

A. Chappell, Centre for Environmental Systems Research, University of Salford, Manchester, UK. (a.chappell@salford.ac.uk)

A. O'Donoghue and A. Robinson, School of Environment & Life Sciences, University of Salford, Manchester M5 4WT, UK.

A. Thomas, Department of Environmental and Geographical Sciences, Manchester Metropolitan University, Manchester M1 5GD, UK.

A. Warren, Department of Geography, University College London, Gower Street, London WC1E 6BT, UK.